

# Atomic structure and charge-density waves of blue bronze $K_{0.3}MoO_3$ ( $20\bar{1}$ ) by variable-temperature scanning tunneling microscopy

Maxim P. Nikiforov,<sup>1,\*</sup> Abdel F. Isakovic,<sup>2,3</sup> and Dawn A. Bonnelli<sup>1</sup><sup>1</sup>Department of Materials Science, University of Pennsylvania, Philadelphia, Pennsylvania 19104-6272, USA<sup>2</sup>Laboratory of Atomic and Solid State Physics, Cornell University, Ithaca, New York 14853-2501, USA<sup>3</sup>NSLS, Brookhaven National Laboratory, Upton, New York, 11973-5000, USA

(Received 27 February 2007; published 23 July 2007)

Blue bronze ( $K_{0.3}MoO_3$ ) has been the focus of a number of scattering, transport, scanning tunneling microscopy (STM), and theoretical studies that have provided insight into the relation between atomic structure and charge-density wave (CDW) formation. However, the full extent of a relation of the CDWs to the atomic lattice and the microscopic origin of CDW pinning are still not completely resolved. In this study STM is used to distinguish the atomic structure and CDWs at the ( $20\bar{1}$ ) surface. Within the STM's spatial resolution, the CDWs are incommensurate with the lattice at midrange temperatures and approach commensurability at low temperatures. Incommensurate CDWs are present on the surface and the degree of the incommensurability between blue bronze lattice and CDW lattice agree well with those determined from bulk scattering techniques.

DOI: 10.1103/PhysRevB.76.033104

PACS number(s): 71.45.Lr, 73.20.-r, 71.20.-b, 68.37.Ef

Complex oxides continue to receive extensive attention due to their rich physical properties arising from electron-phonon interactions, charge and spin ordering, etc. Classic among this class of compounds are the low-dimensional molybdates and tungstates that exhibit charge-density wave (CDW) instabilities.<sup>1</sup> The “blue bronzes” ( $A_{0.3}MoO_3$ , where  $A=K, Rb,$  or  $Tl$ ) in particular have been the focus of a number of scattering,<sup>2-7</sup> transport, scanning tunneling microscopy (STM),<sup>8</sup> and theoretical studies that have provided insight on the relation of atomic and CDW structure and concomitant phase transitions.<sup>1</sup> However several fundamental issues remain. For example, the precise relation between the CDWs and the atomic lattice and the microscopic origin of CDW pinning in these materials are unresolved.

Almost from its invention, STM has been applied to CDW compounds.<sup>8-15</sup> Since STM images the surface density of states near the Fermi level, it can distinguish atomic structure at a surface from spatial variations of charge density when they have a period different from that of the atomic lattice. Attempts to image blue bronzes at room temperature have yielded high spatial resolution.<sup>16-18</sup> Walter *et al.* found no evidence for CDWs at the surface below the Peierls transition temperature  $T_p=180$  K.<sup>8</sup> Recently, Brun *et al.*<sup>19,20</sup> examined the surface of  $Rb_{0.3}MoO_3$  in the temperatures in the range of 63–78 K with STM interpreting the image contrast as superposition of surface topography and CDW. Here we use STM imaging of  $K_{0.3}MoO_3$  to characterize the atomic structure of the surface. We observe CDW modulations that are incommensurate with the lattice at midrange temperatures below Peierls transition and that become indistinguishable from the lattice at lower temperatures near 100 K. We relate these results to the crystallographic structure of  $K_{0.3}MoO_3$ .

Blue bronze (in this case  $K_{0.3}MoO_3$ ) is monoclinic with space group  $C2/m$  and lattice parameters  $a=1.825$  nm,  $b=0.756$  nm,  $c=0.9885$  nm,  $\beta=117.5^\circ$ .<sup>7,21</sup> The structure consists of slabs of distorted  $MoO_6$  octahedra separated by and bonded through K atoms. This layered structure cleaves easily along the ( $20\bar{1}$ ) plane. In the cleavage plane the octahedra

form corner-shared chains along the **b** direction with additional edge-shared octahedral located 0.06 nm lower at one-half of the junctions. Figure 1 illustrates that the ( $20\bar{1}$ ) surface plane contains three different Mo environments. The electron density is higher at the Mo II and Mo III than at the Mo I because the average valence of the former is 5.6, while that of Mo I is 5.75.<sup>22</sup> Consequently, Mo II and Mo III contribute significantly to the density of states at the Fermi level, whereas Mo I does not. At room temperature blue bronze ( $K_{0.3}MoO_3$ ) is a quasi-one-dimensional conductor that undergoes a Peierls transition at  $T_p=180$  K that fully gaps the Fermi surface, resulting in semiconducting behavior well below  $T_p$ . Neutron and x-ray scattering have shown that the CDWs are incommensurate with the atomic lattice below 180 K,<sup>4</sup> with a CDW wave vector  $q_{CDW}$  component along the

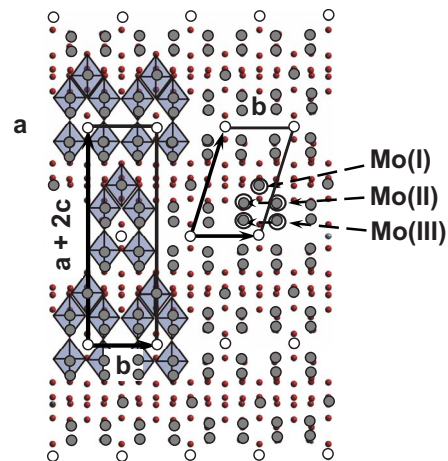


FIG. 1. (Color online) The structure of the  $K_{0.3}MoO_3$  ( $20\bar{1}$ ) surface illustrating three different environments of Mo atoms (white circles are K, gray circles are Mo, small dark gray circles are O; note that K, Mo, and O are drawn not to scale). Mo octahedra are shaded with violet (light gray) color. There are two representations of the surface structure present: (a) traditional (**b**; **a+2c**) and (b) conventional crystallographic (**b**; **112**).

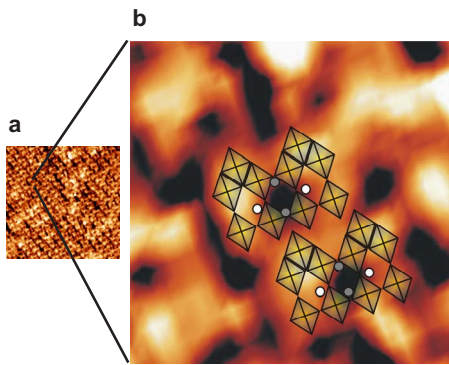


FIG. 2. (Color online) STM image of the room-temperature structure of  $K_{0.3}MoO_3$  ( $20\bar{1}$ ). Bright spots corresponds to the high density of states and could be attributed to Mo octahedra; dark spots correspond to the low density of states corresponding to cooperative effects of potassium atoms on the surface (white circles) and one-half unit cell below the surface (gray circles). (a) Scan size is 21.5 nm. (b) Zoom in from (a) with side size 2.8 nm.

highly conducting  $b^*$  direction of  $\sim 0.26 b^*$ . Grazing incidence x-ray diffraction measurements did not reveal any dependence of the lattice parameter on the depth probed, suggesting that the surface and bulk structures should agree.

Single crystals of blue bronze ( $K_{0.3}MoO_3$ ) were grown in quartz ampoules in the presence of an Ar atmosphere. A mixture of  $MoO_3$ ,  $MoO_2$ ,  $K_2MoO_4$  powders with initial mass ratio 8.04 g : 1.53 g : 2.86 g was hot-pressed into a pellet. The pellet was placed into a quartz ampoule 21.5 cm long and degassed under vacuum, and then the ampoule was back-filled with Ar gas and sealed. The crystals were grown for 10 days at 860 K. The phase composition of the growth was determined by x-ray diffraction.  $I$ - $V$  measurements show an increase in resistance associated with the Peierls transition at  $T_p=180$  K and nonlinear transport at lower temperatures, with a two-probe threshold field of 87 mV/cm at 100 K. This modest threshold field is indicative of a good sample quality, comparable to that obtained by electrochemical growth.

STM images were obtained under UHV conditions ( $P < 10^{-9}$  mBar). The sample was mounted on a degenerately doped silicon base with UHV epoxy (Epotec, H20D) and cleaved under vacuum with a homebuilt attachment. STM measurements were performed with an Omicron VT-25 AFM/STM equipped with a KONTY cryostat. The sample was cooled using liquid  $N_2$ , and its temperature determined with a maximum error of 10 K, the most conservative estimate of the largest possible difference between the sensor and sample surface. The cleaved surfaces became contaminated after 12–18 hours in a background pressure of less than  $10^{-9}$  mBar. Filled state images were acquired with applied biases in the range of 1.5–2 V and currents in the range of 0.1–0.2 nA using a W tip. Only first-order plane fits were performed on the data unless otherwise stated.

Since the density of states near the Fermi level is due to hybridized Mo  $d$  and O  $2p$  states, the STM image contrast is to first order due to the Mo-O octahedra, particularly those of types II and III. Figure 2 compares the room-temperature filled state surface structure to the x-ray diffraction-determined atomic structure, where the Mo-O octahedra have

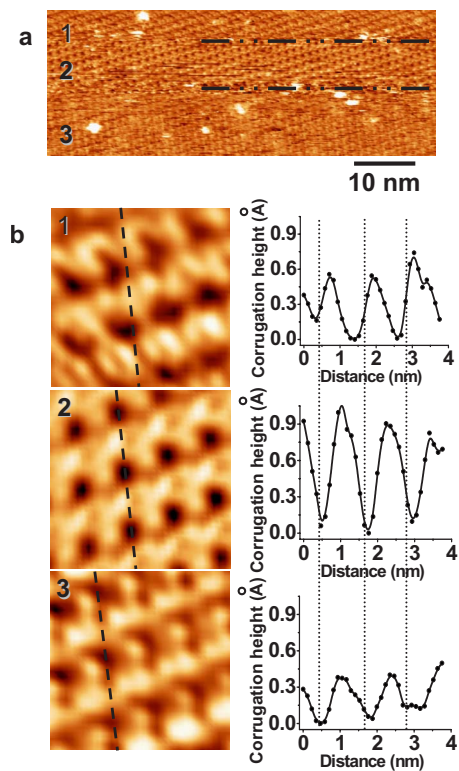


FIG. 3. (Color online) (a) Room-temperature constant current STM image of  $K_{0.3}MoO_3$  demonstrating tip changes during scanning (1, 2, 3). Unit cell resolution is achieved. Sample voltage, +1.5 V; current, 0.15 nA (W tip). (b) Zoom-in of the corresponding parts of image (a) after FFT filtering (image size  $3.8 \times 3.8$  nm).

been aligned with positions of high DOS and the K atoms are aligned with positions of low DOS, as predicted from first principles calculations.<sup>23</sup> STM image contrast results from a convolution of the density of states of the sample and the tip (electronic effect) and from the relative vertical positions of the surface atoms (geometric effect). To relate image contrast to the sample's density of states and atomic structure, the electronic structure of the tip must be either known or unvarying. Most images exhibited uniform and consistent structures. Variations in these structures associated with tip instabilities give insight into the tip's contribution. However, Fig. 3 shows how image contrast patterns changes as the tip structure changes. Because the tunneling current depends exponentially on the sample-tip separation, image contrast is strongly affected by the atom located at the tip's apex. For our W tips, the terminal atom could be W of the pristine tip, O from an oxide layer or acquired from the surface, or Mo acquired from the surface. In region 3, the unit-cell-size corrugations have lateral separation of  $\sim 0.1$  nm and amplitude of  $\sim 0.02$  nm which we attribute to tunneling with a W atom at the tip apex. In region 2, corrugations have the same lateral dimensions but amplitudes of  $\sim 0.06$  nm. Since the DOS of Mo is higher than that of W in the voltage range 0–2 V (Ref. 24) this larger corrugation amplitude suggests the presence of a Mo atom at the tip (the interpretation has been done assuming that DOS of the atom at the tip apex is similar to the DOS of the bulk metal). In region 1, the contrast is completely reversed. This is consistent with an oxygen ter-

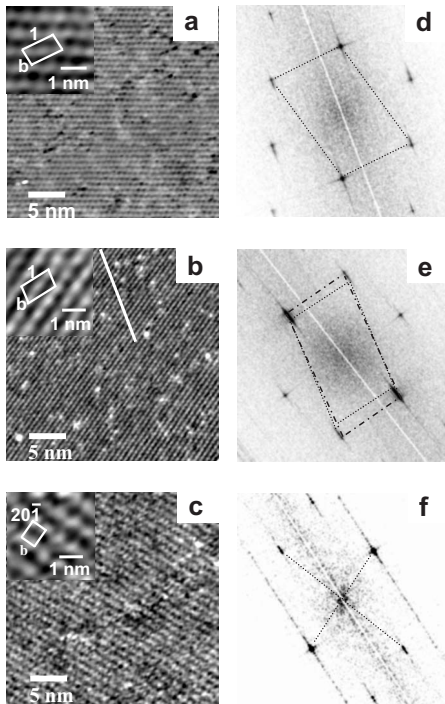


FIG. 4. Variable temperature STM on a vacuum cleaved surface of blue bronze: (a) 300 K, (b) 140 K, and (c) 100 K. FFT of each image is presented on the right-hand side of each one. Splitting the FFT peaks is obvious in image (e). This could be attributed to the formation of incommensurate CDW on the crystal surface. Lowering the temperature (to 100 K) results in structure change shown in the figure at the bottom. Sample voltages: (a) 300 K, +2 V; current, 0.2 nA (W tip); (b) 140 K, sample voltage, +1.5 V; current, 0.2 nA (W tip); (c) 100 K, sample voltage, +1.5 V; current, 0.3 nA (W tip). The line profile in the **b** direction from 4(b) is reproduced in Fig. 5(a).

minated tip, which should have a stronger interaction with the K sites than with the oxide octahedra. Elucidation of the detailed structures of the tip atom clusters requires first principles calculations, but the above considerations allow the stable contrast of region 1 to be associated with the atomic structure as shown in Fig. 2.

For the variable temperature constant current STM measurements in Fig. 4, the “apparent” surface structure changes as the temperature is lowered from 300 K to 100 K. The “apparent” unit cell dimensions determined from real space images and fast Fourier transforms (FFT) of the image contrast are listed in Table I. At 300 K only one periodic structure is present on the (20 $\bar{1}$ ) surface, with lattice vectors  $\mathbf{1}=1.2$  nm and  $\mathbf{b}=0.76$  nm. The modulus of the lattice vector

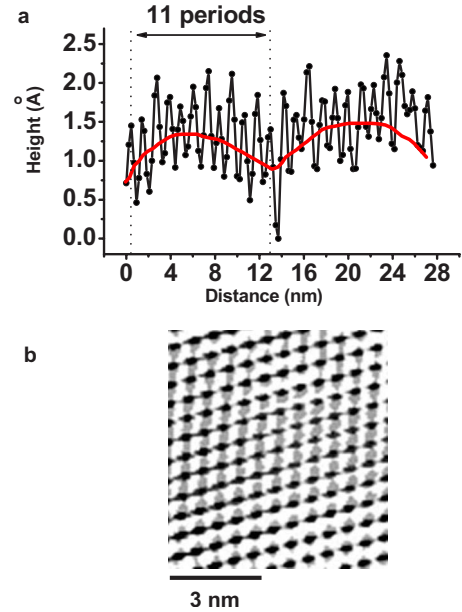


FIG. 5. (Color online) (a) Line profile from Fig. 4(b). The incommensurability between CDW and blue bronze lattices results in long wavelength aliasing on the blue bronze surface. Degree of incommensurability could be calculated from the alias period as  $1/(\text{number of periods}) \cong 9\%$ . (b) The difference in symmetry between surface topography (gray) and charge-density waves (black). The image was created by inverse FFT of the peaks corresponding to surface topography and CDW.

**b** [see inset in Fig. 4(a)] agrees with the corresponding x-ray diffraction-determined lattice parameter in the bulk of 0.756 nm. The modulus of vector  $\mathbf{1}$  matches the known bulk distance between (112) planes, and the angle between vectors  $\mathbf{1}$  and  $\mathbf{b}$  also agree with the bulk angle. At 140 K (below the Peierls transition), two periodic structures are evident from peak splitting in the FFT, Fig. 4(b). One structure has the lattice parameters of the atomic structure at 300 K, consistent with the small change in bulk lattice parameters ( $<1\%$ ) in this temperature range.<sup>22</sup> The second structure is smaller (vector  $\mathbf{1}=1.2$  nm, vector  $\mathbf{b}=0.71$  nm) with slightly different angles between the surface unit vectors (see Table I). We attribute this structure to the CDWs on the surface based on two equivalent analytical procedures elaborated on here. The CDWs can be quantified from STM image data in two ways. First, a profile is extracted from the image along the **b** direction, as shown in Fig. 5(a). The corrugation associated with the CDW is not distinguished in the profile, but the effect of the additional intensity at the atomic sites is clear. The superposition of the two (CDW’ and atomic sites’

TABLE I. The change of surface unit cell dimensions with temperature.

Temperature	Vector $\mathbf{1}$	Vector $\mathbf{b}$	Angle between $\mathbf{1}$ and $\mathbf{b}$
300 K	1.2 nm	0.76 nm	110°
140 K	1.2 nm	0.76 nm	110°
	1.2 nm	0.71 nm	115°
100 K	1.0 nm	0.76 nm	92°

height corrugations) results in an underlying low-frequency component with a period 11 times that of the lattice. This represents a lattice mismatch of about 9%, which agrees with bulk measurements [ $\sim 9\%$  at 140 K (Ref. 14)]. In an alternative approach, the components of the FFT can be separated, reverse transformed, and superimposed, as shown in Fig. 5(b). Here the separation of the two lattices is evident and illustrates mismatch on the order of 10%, along the  $\mathbf{b}$  direction and almost commensurate alignment along the  $\mathbf{a}+\mathbf{b}+2\mathbf{c}$  direction.

On decreasing the temperature to 100 K the additional peaks in the FFT of the STM image are no longer resolved [Figs. 4(c) and 4(f)]. Either the CDWs become commensurate with the atomic lattice or the difference between the two is so small as to be undetectable with the technique.

Previous authors have imaged charge density waves in a similar compound,  $\text{Rb}_{0.3}\text{MoO}_3$ .<sup>15,16</sup> In that case the CDW structure was spatially close to the lattice dimensions that the superposition of the two structures was apparent in superlattice spots in the FFT. In the present case the incommensurate CDW are imaged directly. We suggest that the superlattice spots are not as apparent in our study due to the higher temperature at which the CDWs were imaged. Alternatively, a recent analysis by Canadell and collaborators<sup>25</sup> of a similar

compound  $\text{Rb}_{0.3}\text{MoO}_3$ , indicates that a sensitivity of a detection of alkali-metal atoms may play a role in the interpretation of images.

In summary, the CDW phase transition was observed on the  $\text{K}_{0.3}\text{MoO}_3$  surface with *in situ* variable temperature STM. The atomic structure at the surface exhibited the lattice parameters consistent with those of the bulk at all temperatures. Incommensurate CDWs were present on the surface and the degree of incommensurability with the atomic lattice was determined and found to be in a good agreement with those determined from bulk scattering techniques.

Two of the authors (D.A.B. and M.P.N.) acknowledge support from NSF MRSEC Grant No. DMR05-20020 and the Nano/Bio Interface Center NSEC Grant No. DMR-0425780. One of the authors (A.F.I.) acknowledges M. Weathers and F. DiSalvo for helpful communication regarding the characterization of blue bronze crystals. The work at Cornell was supported in part through NSF Grant No. DMR04-05500. The authors acknowledge R. E. Thorne for providing samples. NSLS-BNL is supported by the U.S. Department of Energy, Office of Science, Office of Basic Energy Sciences, under Contract No. DE-AC02-98CH10886.

\*Corresponding author. maximn@seas.upenn.edu

<sup>1</sup>C. Schlenker, *Low Dimensional Electronic Properties of Molybdenum Bronzes and Oxides* (Kluwer, Dordrecht, 1989).

<sup>2</sup>J. P. Pouget, C. Noguera, A. H. Moudden, and R. Moret, *J. Phys. IV* **46**, 1731 (1985).

<sup>3</sup>G. Gruner and A. Zettl, *Phys. Rep.* **119**, 117 (1985).

<sup>4</sup>R. M. Fleming, L. F. Schneemeyer, and D. E. Moncton, *Phys. Rev. B* **31**, 899 (1985).

<sup>5</sup>X. M. Zhu, R. Moret, H. Zabel, I. K. Robinson, E. Vlieg, and R. M. Fleming, *Phys. Rev. B* **42**, 8791 (1990).

<sup>6</sup>S. Rouziere, S. Ravy, J. P. Pouget, and S. Brazovskii, *Phys. Rev. B* **62**, R16231 (2000).

<sup>7</sup>W. J. Schutte and J. L. Deboer, *Acta Crystallogr., Sect. B: Struct. Sci.* **49**, 579 (1993).

<sup>8</sup>U. Walter, R. E. Thomson, B. Burk, M. F. Crommie, A. Zettl, and J. Clarke, *Phys. Rev. B* **45**, 11474 (1992).

<sup>9</sup>R. V. Coleman, B. Drake, P. K. Hansma, and G. Slough, *Phys. Rev. Lett.* **55**, 394 (1985).

<sup>10</sup>C. G. Slough, B. Giambattista, A. Johnson, W. W. McNairy, and R. V. Coleman, *Phys. Rev. B* **39**, 5496 (1989).

<sup>11</sup>Z. X. Dai, C. G. Slough, and R. V. Coleman, *Phys. Rev. Lett.* **66**, 1318 (1991).

<sup>12</sup>R. V. Coleman, Z. Dai, C. G. Gong, C. G. Slough, and Q. Xue, *J. Vac. Sci. Technol. B* **12**, 1801 (1994).

<sup>13</sup>H. J. Dai and C. M. Lieber, *J. Phys. Chem.* **97**, 2362 (1993).

<sup>14</sup>E. Meyer, R. Wiesendanger, D. Anselmetti, H. R. Hidber, H.-J. Güntherodt, F. Levy, and H. Berger, *J. Vac. Sci. Technol. A* **8**, 495 (1990).

<sup>15</sup>E. Meyer, D. Anselmetti, R. Wiesendanger, H.-J. Güntherodt, F. Levy, and H. Berger, *Europhys. Lett.* **9**, 695 (1989).

<sup>16</sup>D. Anselmetti, R. Wiesendanger, H.-J. Güntherodt, and G. Gruner, *Europhys. Lett.* **12**, 241 (1990).

<sup>17</sup>J. Heil, J. Wesner, B. Lommel, W. Assmus, and W. Grill, *J. Appl. Phys.* **65**, 5220 (1989).

<sup>18</sup>G. Rudd, D. Novak, D. Saulys, R. A. Bartynski, S. Garofalini, K. V. Ramanujachary, M. Greenblatt, and E. Garfunkel, *J. Vac. Sci. Technol. B* **9**, 909 (1991).

<sup>19</sup>C. Brun, J. C. Girard, Z. Z. Wang, J. Dumas, J. Marcus, and C. Schlenker, *J. Phys. IV* **131**, 203 (2005).

<sup>20</sup>C. Brun, J. C. Girard, Z. Z. Wang, J. Marcus, J. Dumas, and C. Schlenker, *Phys. Rev. B* **72**, 235119 (2005).

<sup>21</sup>J. Graham and A. D. Wadsley, *Acta Crystallogr.* **20**, 93 (1966).

<sup>22</sup>M. Ghedira, J. Chenavas, M. Marezio, and J. Marcus, *J. Solid State Chem.* **57**, 300 (1985).

<sup>23</sup>J. L. Mozos, P. Ordejon, and E. Canadell, *Phys. Rev. B* **65**, 233105 (2002).

<sup>24</sup>D. A. Papaconstantopoulos, *Handbook of the Band Structure of Elemental Solids* (Plenum, New York, London, 1986).

<sup>25</sup>E. Machado-Charry, P. Ordejon, E. Canadell, C. Brun, and Z. Z. Wang, *Phys. Rev. B* **74**, 155123 (2006).